AAS 10-202

SURVEY OF ORBIT NON-LINEARITY EFFECTS IN THE SPACE CATALOG

Sergei Tanygin,[*] and Vincent T. Coppola[†]

Accurate ephemeris and error covariance propagation are critical for space situational awareness and conjunction analysis which became especially important in light of recent conjunction events. Various factors affecting propagation accuracy, such as accuracy of the initial state, force modeling, and covariance realism, have been examined in the past. This paper focuses on the cumulative effects that non-linearity of the error propagation has on predicted ephemerides of the objects in the US space catalog over periods of several days. In particular, the paper examines the effect of non-linearity on conjunction events including differences in times of closest approach, minimum ranges as well as true and maximum probabilities of collision.

INTRODUCTION

Improving space situational awareness and conjunction analysis in particular has taken on a new urgency due to a series of recent events, such as 2007 Chinese anti-satellite (ASAT) test, the 2008 intercept of USA 193 and, of course, the collision of Iridium 33 and Cosmos 2251.[1] Predicting possible conjunctions requires propagation of all available state vectors which currently number over 19,000 in the US space catalog.[2] A conjunction is typically examined around the time of closest approach (TCA) and is quantified either by the miss distance at TCA or by some measure of probability of collision.[3,4,5,6,7] Accuracy of conjunction analysis and consequently correctness of operational decisions that are based on it depend strongly on the ability to accurately predict the most likely ephemerides[‡] for all objects involved. We can identify three factors that influence prediction accuracy:

1) the accuracy of the initial state and error covariance generated by the orbit determination (OD) process
2) the accuracy of the dynamical model (consistent with the OD process) used to propagate the initial state and error covariance
3) the effect of nonlinearity on the propagated error distribution

The first two factors lie outside of the scope of this paper and have been carefully examined by other authors.[8,9,10,11] The effect of nonlinearity has also been studied by others who proposed various nonlinearity metrics.[12,13,14] In this paper we apply some of these metrics to the entire US Space Catalog and examine the results. We run the OD process using simulated measurements and then propagate the initial state and error covariance using the full dynamical model. We calculate deviations of the expected error due to the nonlinearity of propagation for all objects in the US space catalog. We trend results for various classes of orbits

[*] Sr. Astrodynamics Specialist, Analytical Graphics, Inc., 220 Valley Creek Blvd., Exton, PA 19341.
[†] Sr. Astrodynamics Specialist, Analytical Graphics, Inc., 220 Valley Creek Blvd., Exton, PA 19341.

[‡] For true probability of collision, accurate prediction of the statistical distribution of the errors is also required for all objects involved.

and compute measures of non-linearity as functions of elapsed time. Finally, we evaluate the effect that deviations of the expected error have on conjunction geometries and probabilities of collision.

THE SECOND ORDER EFFECT DURING ORBIT ERROR PROPAGATION

The second order effect arises due to nonlinearity of the orbit error propagation. This is a response of the future error due to the terms that are second order in the initial error. Consider state error transition to second order (see References 13 and 14)

$$\delta\mathbf{s} = \boldsymbol{\Phi}\delta\mathbf{s}_0 + \frac{1}{2}\begin{bmatrix} \delta\mathbf{s}_0^{\mathrm{T}}\boldsymbol{H}_1\delta\mathbf{s}_0 \\ \ldots \\ \delta\mathbf{s}_0^{\mathrm{T}}\boldsymbol{H}_N\delta\mathbf{s}_0 \end{bmatrix} \tag{1}$$

where $\delta\mathbf{s}$ is the state error at time t, $\delta\mathbf{s}_0$ is the initial state error at time t_0, $\boldsymbol{\Phi}$ is the state error transition matrix, and $\boldsymbol{H}_i$, $i = 1, 2, ..., N$ are the state error transitive Hessians, one for each element of the state. It follows immediately that in general the expectation of the future error is non-zero, $\delta\hat{\mathbf{s}} \equiv E\{\delta\mathbf{s}\} \neq \mathbf{0}$, even if the expectation of the initial error is, $\delta\hat{\mathbf{s}}_0 \equiv E\{\delta\mathbf{s}_0\} = \mathbf{0}$. Indeed, from Equation (1) we obtain

$$\delta\hat{\mathbf{s}} = \frac{1}{2}\begin{bmatrix} tr\{\boldsymbol{P}_0\boldsymbol{H}_1\} \\ \ldots \\ tr\{\boldsymbol{P}_0\boldsymbol{H}_N\} \end{bmatrix} \tag{2}$$

which should be added to the propagated state $\mathbf{s}$ in order for it to represent the expected state $\hat{\mathbf{s}}$ to second order: $\hat{\mathbf{s}} = \mathbf{s} + \delta\hat{\mathbf{s}}$.

Another way to evaluate this effect is to consider the differential equation of the state:

$$\dot{\mathbf{s}} = \mathbf{f}(\mathbf{s}(t)). \tag{3}$$

To second order the state error differential equation becomes

$$\delta\dot{\mathbf{s}} = \boldsymbol{F}\delta\mathbf{s} + \frac{1}{2}\begin{bmatrix} \delta\mathbf{s}^{\mathrm{T}}\boldsymbol{G}_1\delta\mathbf{s} \\ \ldots \\ \delta\mathbf{s}^{\mathrm{T}}\boldsymbol{G}_N\delta\mathbf{s} \end{bmatrix} \tag{3}$$

where $\boldsymbol{F}$ is the Jacobian, and $\boldsymbol{G}_i$, $i = 1, 2, ..., N$ are the Hessians of that equation, one for each element of the state. Then the expectation $\delta\hat{\dot{\mathbf{s}}} \equiv E\{\delta\dot{\mathbf{s}}\}$ is obtained in a manner similar to getting Equation (2) from Equation (1)[15]

$$\delta\hat{\dot{\mathbf{s}}} = \frac{1}{2}\begin{bmatrix} tr\{\boldsymbol{P}\boldsymbol{G}_1\} \\ \ldots \\ tr\{\boldsymbol{P}\boldsymbol{G}_N\} \end{bmatrix} \tag{4}$$

This correction is included in the nonlinear differential equation of the state

$$\hat{\dot{\mathbf{s}}} = \mathbf{f}(\hat{\mathbf{s}}(t)) + \delta\hat{\dot{\mathbf{s}}} \tag{5}$$

solution of which yields the expected state $\hat{\mathbf{s}}$ corrected to second order.

The Keplerian transitive Hessians $\boldsymbol{H}_i$ are given in Reference 14 and the Hessians $\boldsymbol{G}_i$ of the two-body dynamics can be found in Reference 15. It is argued in Reference 14 that nonlinearity contributions from higher order error terms are progressively more dominated by the Keplerian dynamics and that it is therefore reasonable to combine the Keplerian second order error effects with the full non-Keplerian dynamics.

GENERATION OF SIMULATED DATA FOR THE SURVEY

The difficulty in assessing the space object catalog is its unavailability: the only public source of data consists of TLEs (i.e., two-line element sets) for a (large) subset of the objects being tracked. The TLEs are not highly accurate, nor do they provide covariance information, so they are not satisfactory for our purposes. However, the public TLE catalog does provide a starting point for producing a representative space object catalog.

Ephemeris and Covariance Generation

We cannot use the actual space object catalog for our analysis because the data is not made publically available. We will instead create representative space object catalog using the publically available TLEs from 25 Jan 2010 as a starting point. That catalog consisted of 14,153 space objects.

For each object in the catalog, we used SGP4 to propagate the object's TLE to the epoch 24 Jan 2010 00:00:00 to obtain an initial position and velocity of the object. We then used orbit determination software (in our case, ODTK) to simulate range measurements over a one day period (24-25 Jan 2010 00:00:00) from 8 AFSCN sites. We then ran a sequential estimation filter to process the simulated measurements over one day, thereby obtaining the object's position, velocity, and covariance for the epoch 25 Jan 2010 00:00:00. This state was then propagated forward in time for a duration of 5 days (25-30 Jan 2010 00:00:00) with the covariance evolving according to the variational equations. The result is a high fidelity ephemeris for each object, complete with numerically integrated position-velocity covariance. The orbit determination process was used to compute an accurate position-velocity covariance, complete with position-velocity correlations, which are not known *a priori*.

The force model settings included a 21x21 EGM-96 gravitational field, solar and lunar third body perturbations, atmospheric drag using the CIRA 1972 density model, and solar radiation pressure. The only tuning of the force model was the removal of drag for sufficiently high orbits and the removal of solar radiation pressure for lower orbits. All objects were assigned the same mass, Cd and Cr properties.

The simulated data was created to provide a measurement rich environment with many observations for every pass of each object. The resulting covariance at the epoch 25 Jan 2010 00:00:00 was smaller (a few meters of 1σ position error for a LEO) than would be expected of the actual catalog, since the simulator provided an abundance of observations that are not normally available for each object in the catalog. We increased the initial covariance matrices by a factor of 25 (a 5-fold increase of 1σ errors) and which resulted in the typical covariance size for a LEO on the order of 10 m, still an excellent OD result for such an object.

Of course, the resulting ephemeris does not match the original TLE, nor is it an accurate ephemeris for the actual space object itself. It is not our intent to produce accurate for the actual space catalog (which cannot be obtained from just a TLE anyway). Rather, our intent was to produce a representative space object catalog consisting of high fidelity data (i.e., numerically integrated trajectories with corresponding representative position-velocity covariance).

Addition of the Second Order Correction

A reference trajectory was numerically integrated for each of the 14,153 objects where the second order correction to the expected orbit was not considered. We then created a corrected trajectory for each object

that included the second order effect (see Equation 5). We include RMS (square root of the trace) of the initial position covariance for various classes of orbits in Table 1.

Catalog Classification

We introduced a set of orbit classes in order to categorize large amounts of data and better understand the results. After examining the TLEs, we found 13 orbit classes to be descriptive for our purposes, see Table 1.

The vast majority of objects are classified as LEO Circular, indicating near circular low Earth orbits. The next largest groups are GEO (geosynchronous orbits) and Eccentric (eccentric orbits that do not cross the geo belt). Super GEO are super-synchronous orbits (i.e., orbits above the geosynchronous belt). GTO refers to an orbit that crosses the geosynchronous belt; GTO High refers to an orbit much higher than the geosynchronous belt; GTO Low refers to an orbit that passes through low Earth orbit as well; GTO Medium refers to an orbit passing through medium altitudes (between LEO and GEO).

Table 1. Catalog Classification.

Orbit Class	Definition n = Mean Motion (revs/day), e = Eccentricity, a = Semi-major Axis (Earth Radii), r_a = Radius of Apogee (Earth Radii), r_p = Radius of Perigee (Earth Radii), a_p = Perigee Altitude (km), i = Inclination (deg)	Range of Values for Initial Position Covariance RMS Based on Simulated Tracking (m)	Number of Objects
LEO Circular	$n > 4$, $a_p > 300$, $e \le 0.05$	5 - 126	10,606
LEO	$n > 4$, $0.05 < e < 0.2$	6 - 37	718
LEO High Drag	$200 \le a_p < 300$	13 - 233	29
LEO Decaying	$a_p \le 200$	25 – 129, 1080	9
MEO Circular	$n \le 4$, $e < 0.05$	13 – 28, 51	223
GEO	$n \le 1.1$, $a < 6.8$	18 – 80, 150	991
Super GEO	$a \ge 6.8$, $e < 0.2$	28 - 62	30
Eccentric Low	$n > 4$, $0.2 \le e < 0.5$	7 - 16	179
Eccentric	$e \ge 0.5$	9 – 93, 209, 539	906
Eccentric Super High	$a \ge 6.8$, $e \ge 0.2$	30 - 336	25
GTO Low	$r_p \le 2.0$, $r_a \ge 6.0$, $e \ge 0.5$, $\lvert i \rvert \le 10$	10 - 48	237
GTO Medium	$n \le 4$, $0.2 \le e < 0.5$	16 - 48	39
GTO High	$r_a \ge 7.0$, $e \ge 0.5$	12 - 63	161
Total:			14,153

ANALYSIS METRICS FOR THE SURVEY

Several analysis metrics were considered. One group of metrics is used to assess the absolute and relative significance of the second order effect for the entire catalog. In particular, we look for correlations of the effect with different classes of orbits and with different levels of uncertainty. Another group of metrics is used to quantify the effect for a selected set of conjunction events. In this case, we evaluate the effect on the TCA, miss distance at TCA and its uncertainty, and on the probabilities of collision.

Table 2. General Trends and Dependencies of the Second Order Correction.

Orbit Class	Dependency			Maximum Correction Distance after 1 Period (m)	Maximum Correction Distance after 12 hrs (m)
	Initial Position Covariance	Eccentricity	Mean Motion		
LEO Circular	Strong	None	Strong	< 1.1	< 9
LEO	Strong	None	Strong with exceptions	< 0.08	< 1
LEO High Drag	Initially strong	None	Strong with exceptions	< 4	< 25
LEO Decaying	Not enough evidence	Not enough evidence	Not enough evidence	< 3	< 322
MEO Circular	Strong	None	None	< 0.03	< 0.02
GEO	Strong with some exceptions	None	None	< 0.7	< 0.4
Super GEO	Moderate	None	None	< 0.07	< 0.03
Eccentric Low	Weak	None	None	< 4	< 232
Eccentric	None	None	None	< 19	< 20
Eccentric Super High	Not enough evidence	Not enough evidence	Not enough evidence	< 11	< 0.17
GTO Low	None	Weak with exceptions	Weak with exceptions	< 4	< 4
GTO Medium	None	None	None	< 0.1	< 0.1
GTO High	None	Moderate with exceptions	None	< 4	< 4

The Second Order Effect on the Catalog – General Trends

For each object in the catalog we computed the difference between its corrected and reference trajectories. In the survey based on simulated data, we are more interested in general trends than in the exact numerical differences for individual objects. In particular, we look for dependencies between the evolution of the correction over time and the initial state and error covariance. We found that the general trends can be identified for each orbit class and that they typically depend on the initial covariance, eccentricity and mean motion. These trends are summarized in Table 2. The table includes the maximum correction distance recorded for each object after one orbit period and after a period of 12 hours. The table shows that the major-

ity of near circular orbits exhibits strong dependency of the correction on the initial covariance. These results are illustrated in Figures 1 and 2.* Super GEO and Eccentric Low orbit classes exhibit moderate to weak dependency shown in Figures 3 and 4. Eccentric class in particular demonstrates significant disparity in the growth of the correction for comparable initial covariances. One might expect that this behavior can be explained by different eccentricities of orbits in that class but we found no reliable evidence of that (see Table 2 and Figure 5). In fact eccentricity alone was not found to be a dominant factor for any of the orbit classes. It appears that significant eccentricity is necessary but not sufficient to generate rapid growth of the correction. Most likely it requires some combination of both the eccentricity and the initial covariance. Results included in Table 2 also indicate that the majority of LEO objects, in particular in near circular orbits, exhibit strong dependency on mean motion (for example, see Figure 6).

The Second Order Effect on the Catalog – Exceptional Cases

It can be expected that over time the second order effect will force the corrections to become too large. "Too large" in this context refers to the situation when accurate propagation of the state error requires terms higher then the second order in the expansion of the force model. In general the second order contribution over time should transition from insignificant, to significant and accurate, to, finally, significant but inaccurate. Of course, by the time the contribution becomes inaccurate, the Gaussian assumptions also begin to breakdown and we can no longer rely on the first two moments of the error distribution. Thus, we should not propagate the state and its error covariance beyond the time when the second order contribution becomes inaccurate. Nor should we make any risk assessments about possible close approaches if corrections to either of the trajectories involved become too large. We propose several metrics for determining when that happens in the subsequent sections of the paper. In this section we identify several objects in the catalog for which this situation became quite evident using a simple criterion that the maximum correction distance grew larger than 1 km (see Table 3).

It is clear from Table 3 that objects with higher eccentricities or with faster growth of the error covariance have a greater chance of quickly evolving exceptionally large corrections. Some of these corrections are so large (e.g. see Eccentric Object 26898 with 6920.87 km correction) that it is not surprising when these objects either decay or become hyperbolic before reaching the intended 5 day mark. It is also clear that for other objects in this table it is more difficult to determine whether the correction is too large to be accurate (e.g. see Eccentric Object 32780 with 2.29 km correction). This difficulty highlights the need for more robust metrics for determining when the correction becomes too large and, therefore, determining when further propagation and collision risk assessment are imprudent. These metrics are developed later in this paper after we consider the second order effect on close approaches for cataloged objects.

The Second Order Effect on Close Approaches

Any effect that significantly changes trajectories of the cataloged objects may also significantly impact close approaches. In order to assess the impact of the second order corrections, we computed conjunctions for all possible pairs of objects in the catalog (i.e., an all-on-all computation) over a 5-day ephemeris span. For the catalog of 14,153 objects, just over 100 million pairs are considered. The computation can be performed in just over 2.1 hours on an 8-core 64-bit personal computer (see Reference 2 for a discussion of the methodology used to perform the computation). We used a range criterion to detect events below a 50 km range threshold for GEO, Super GEO, GTO, and Eccentric Super High objects and a 5 km threshold for all others.

* In all figures in this section we use the following notation for metrics recorded for each object: the earliest recorded metric, e.g. metric after 1 orbit period or after 12 hours, is denoted by a circle, the latest recorded metric, e.g. metric after maximum number of recorded periods, is denoted by a triangle, metrics recorded at intermediate times are denoted by points.

Table 3. Exceptional Cases of the Second Order Correction after up to 5 days.[*]

Object Class	Object	Elapsed Time	Maximum Correction Distance	Exceptional / Total
LEO Circular	27498	4 days	2.98 km	2 / 10,606
	35694	4 days	214.94 km	
LEO High Drag	28099	32 Periods	5.17 km	5 / 29
	33445	32 Periods	122.35 km	
	33755	32 Periods	1.14 km	
	34602	32 Periods	2.87 km	
	35695	32 Periods	1.11 km	
LEO Decaying	25814	22 Periods	270.66 km	4 / 9
	26640	22 Periods	4.19 km	
	29908	22 Periods	2.11 km	
	32007	22 Periods	102.54 km	
Eccentric Low	28083	17 Periods	4.24 km	4 / 179
	28476	17 Periods	4.05 km	
	29602	17 Periods	74.04 km	
	32385	17 Periods	264.19 km	
Eccentric	17134	10 Periods	4.92 km	5 / 906
	25812	10 Periods	82.44 km	
	26898	10 Periods	6920.87 km	
	32780	10 Periods	2.29 km	
	34943	10 Periods	11.71 km	
GTO Low	32770	11 Periods	6.85 km	2 / 237
	35497	11 Periods	13.18 km	
GTO High	21709	6 Periods	545.36 km	1 / 161
Total:				23 / 14,153

The assessment of the reference trajectories produced 50,705 events; the assessment of the corrected trajectories produced 50,699 events. The reference set included 17 events not present in the corrected set; the corrected set included 11 events not found in the reference set; both sets found the same 50,688 events, though for some events the characteristics of the event (miss distance, TCA) were significantly different.

[*] Elapsed time for each orbit class in the table may be further limited by objects that decayed or became hyperbolic due to exceptionally high 2nd order effect.

Many of the cases involving missing events included an object whose trajectory changed drastically due to the correction — usually by tens of kilometers (if not more). As mentioned earlier, most likely such a correction is too large indicating that the event (as the trajectory itself at that point) is not reliable.

For the 50,688 similar events, we compared the TCA range as computed by the reference and the corrected sets. The largest TCA range difference was 6.0 km, caused by a GTO Low object with the correction distance reaching up to 22 km over the course of 5 days. However, the reference TCA range for the event was 36 km so that the difference represented a 17% difference over the reference range. The largest percentage difference was 36% involving an Eccentric Low object with the correction distance reaching up to 6.3 km over 5 days. For this event the nominal TCA range of 2.9 km was reduced to 1.9 km when the second order corrections were considered. A summary of the results are shown in Table 4.

Table 4. Summary of the Close Approach Differences due to the Second Order Effects.

Close Approach Event	Occurrences
TCA range difference > 1 km	2
1 km > TCA range difference > 100 m	19
100 m > TCA range difference > 10 m	51
10 m > TCA range difference > 1 m	280
TCA range difference < 1 m	50,336
TCA range difference / TCA range > 10%	3
10% > TCA range difference / TCA range > 1%	11
1% > TCA range difference / TCA range > 0.1%	81
TCA range difference / TCA range < 0.1%	50,593

From Table 4 it is clear that in the vast majority of events the second order corrections produced negligible updates to the TCA range. The same can be said for the maximum and true probability metrics, since they depend heavily on the TCA range. As expected, in cases where the TCA range was not updated significantly, neither was the TCA time itself. Even in cases of large TCA range updates, the TCA time was updated by less than 1 second---usually much less.

Nonetheless, there are cases in which the second order corrections were found to be relatively small while still producing a significant difference in the close approaches, see Table 5. Object 35780 (Cosmos 2251 debris) is a LEO Circular object in an inclined orbit (a = 7000 km, e = 0.0217, i= 73.93 deg); the correction distance is less than 1 meter at conjunction. Object 34712 (Breeze-M debris) is an Eccentric object (a = 14007 km, e = 0.5241, i = 46.06 deg); its correction distance at conjunction is 83 m. The covariance for both objects is dominated by the along track component, with a 1σ value of 1.7 km for 35780 and 15.7 km for 34712. The conjunction occurs near perigee.

Note that the inclusion of the corrections moves the TCA by 5 ms and results in a closer approach by 30%, from 98.8 m to 68.7 m, though the collision probability decreases 50%. It appears that, though rare, the second order corrections can produce a meaningful, yet different, result---one that may argue for a different mitigation strategy than would otherwise be the case.

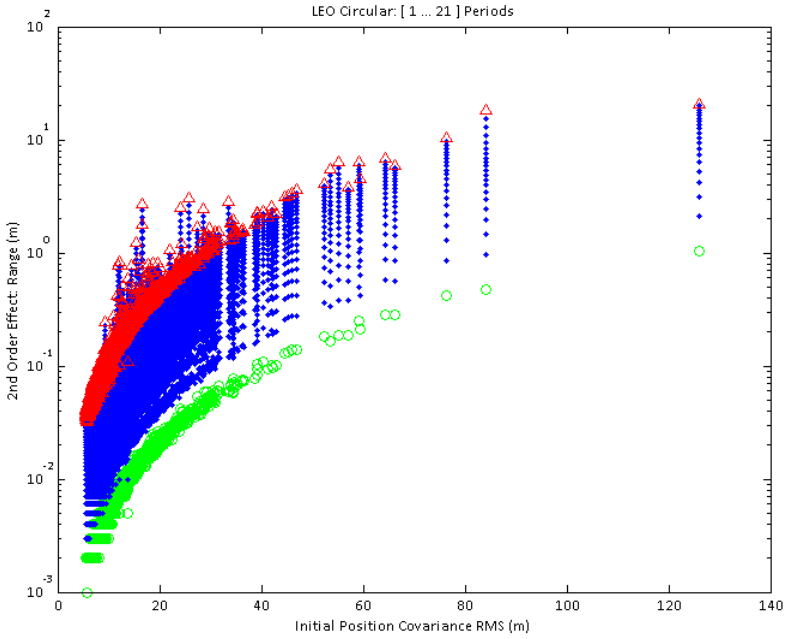

Figure 1. Strong Dependency of LEO Circular Class on the Initial Covariance.

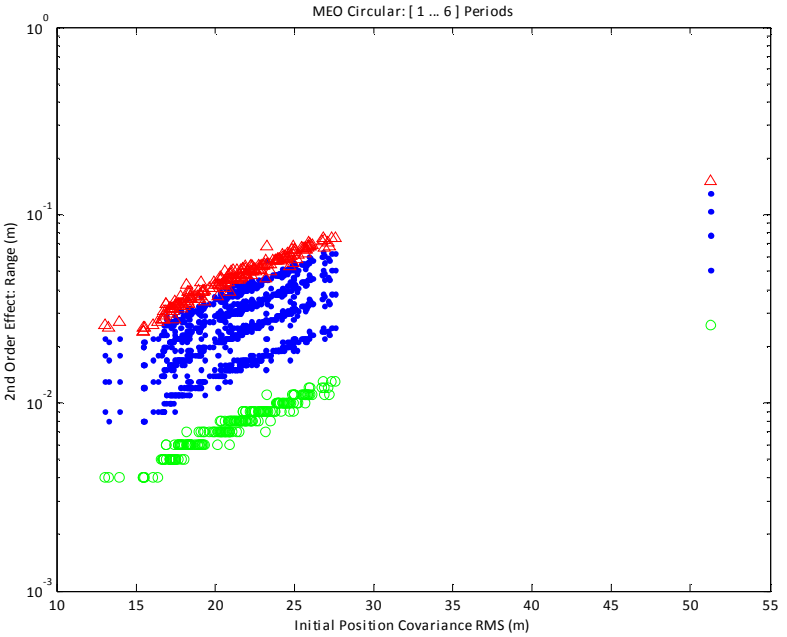

Figure 2. Strong Dependency of MEO Circular Class on the Initial Covariance.

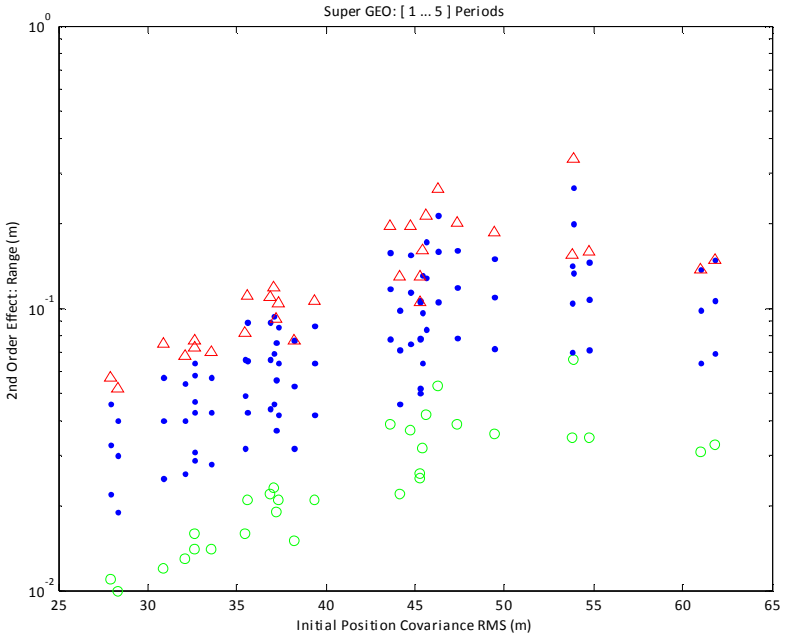

Figure 3. Moderate Dependency of Super GEO Class on the Initial Covariance.

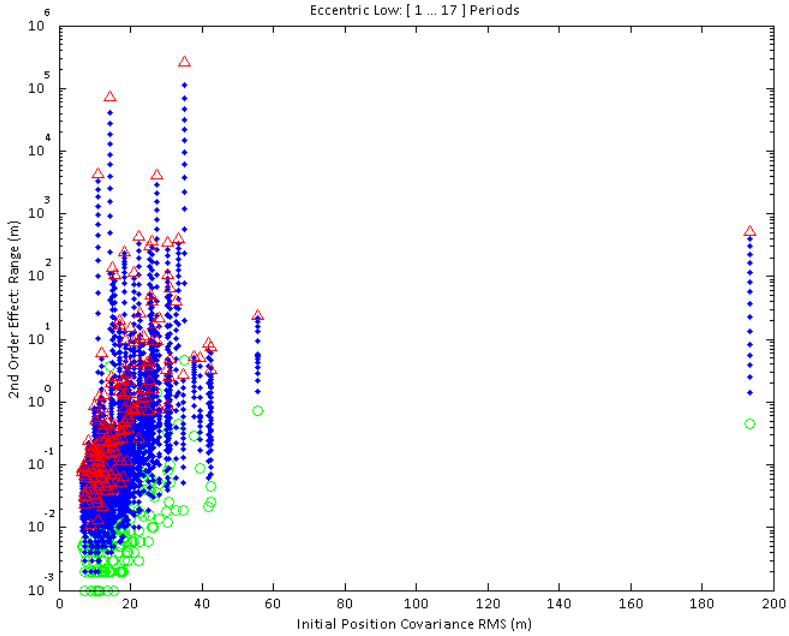

Figure 4. Weak Dependency of Eccentric Low Class on the Initial Covariance.

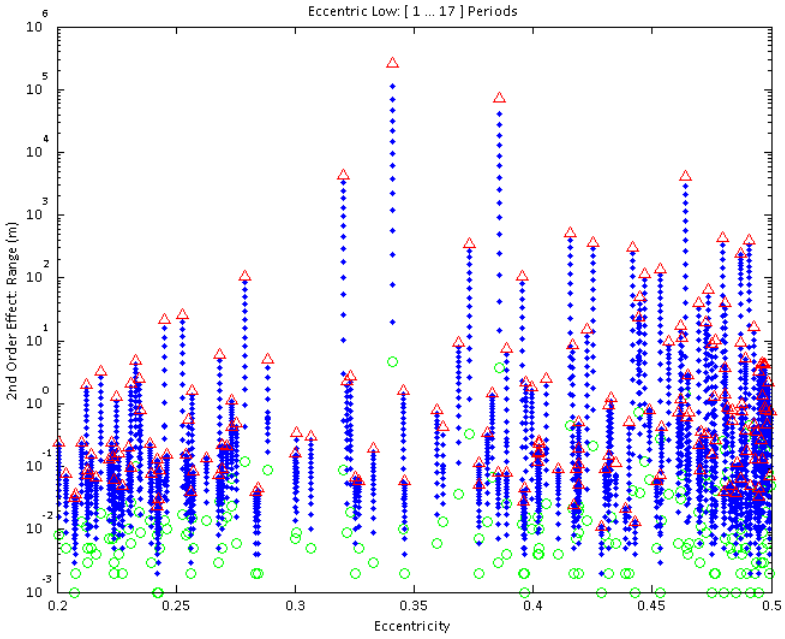

Figure 5. Inconclusive Dependency of Eccentric Low Class on Eccentricity.

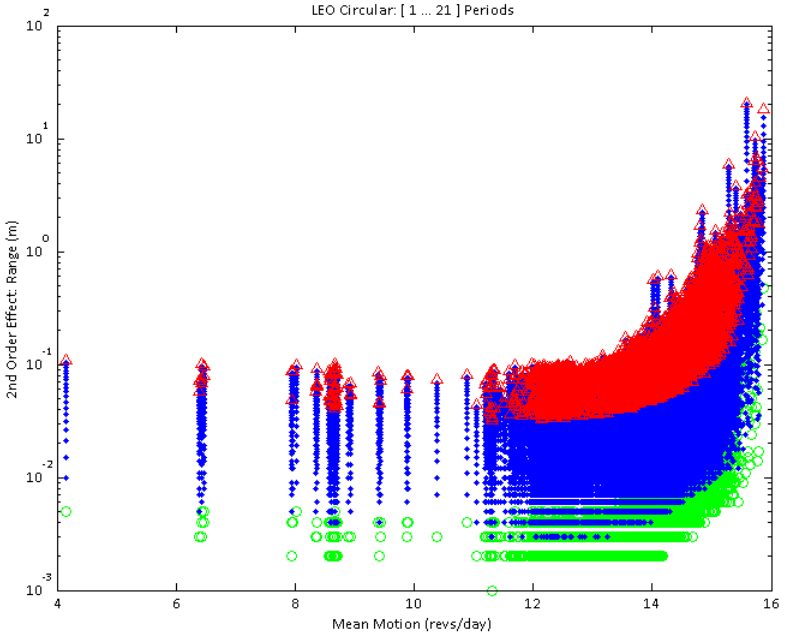

Figure 6. Strong Dependency of LEO Circular Class on Mean Motion.

Table 5. Conjunction Between Objects 35780 (LEO Circular) and 34712 (Eccentric) on 28 Jan 2010.

	Reference Ephemeris	With 2nd Order Effects	Difference
TCA	05:07:55.906	05:07:55.901	-5.0 ms
TCA Range	98.8 m	68.7 m	-30.1 m
Approach Angle	113.26	113.26 deg	0.0 deg
Range Uncertainty	7.3 km	5.8 km	-1.5 km
Collision Probability	4.1e-6	2.1e-6	-2.0e-6

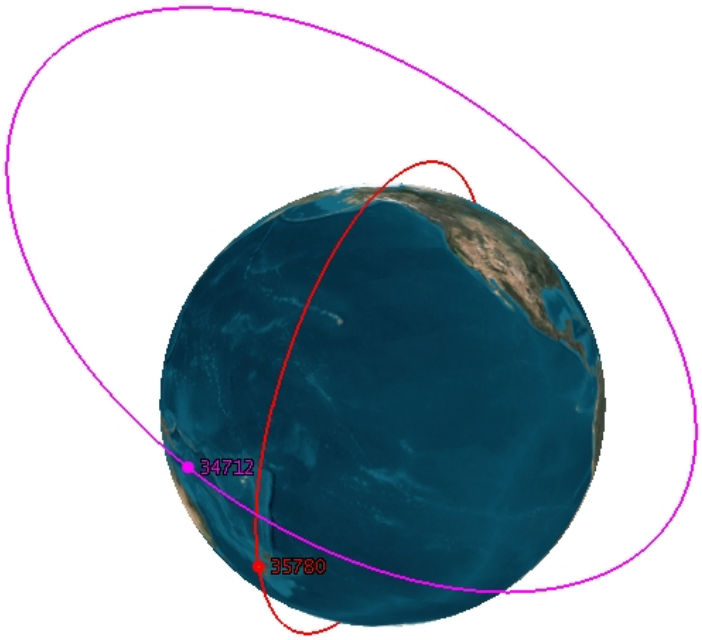

Figure 7. Objects 34712 and 35780 Shown 4 Minutes Prior to TCA.

PREDICTION LIMITS AND ACCURACY OF THE SECOND ORDER CORRECTION

In previous sections we highlighted the need for a more robust approach to determining when the second order correction becomes inaccurate and, therefore, when further propagation and close approach analysis are imprudent. In this section we develop several metrics to fill this need. Then we test them on one of the exceptional cases listed in Table 3.

The Fractional Acceleration Metric

This metric proposed in Reference 16 estimates instantaneous significance of the second order acceleration from Equation (4) by comparing it to the two-body acceleration[16]

$$\delta_a \equiv \frac{\left|\delta\hat{\hat{\mathbf{s}}}\right|}{\left|\mu / r^2\right|} \tag{6}$$

where μ is the gravitational parameter and r is the magnitude of the position vector (see Reference 16 for details on computing $\delta\hat{\hat{\mathbf{s}}}$ for this metric). The larger this metric the more significant is the second order contribution and when it becomes larger then some user-defined threshold the resulting correction at this and all subsequent times may be considered inaccurate. It is perhaps reasonable to set the threshold lower than any of the non-two-body accelerations included in the dynamical model.

The Mahalanobis Relative Position and Relative Velocity Metrics

The Mahalanobis distance is often used to evaluate statistical significance of deviations. It was proposed as a possible measure of nonlinearity in Reference 14. We can apply it here to determine relative significance of the second order position and velocity corrections. The relative position and relative velocity metrics are

$$\delta_r \equiv \Delta\mathbf{r}^{\mathrm{T}} \boldsymbol{P}_{rr}^{-1} \Delta\mathbf{r} \tag{7}$$

and

$$\delta_v \equiv \Delta\mathbf{v}^{\mathrm{T}} \boldsymbol{P}_{vv}^{-1} \Delta\mathbf{v} \tag{8}$$

where $\Delta\mathbf{r}$ is the position correction vector and $\Delta\mathbf{v}$ is the velocity correction vector computed as the difference between the corresponding corrected and reference trajectories. Also, where $\boldsymbol{P}_{rr}$ and $\boldsymbol{P}_{vv}$ are the position and velocity portions of the error covariance matrix, respectively. Geometrically, these metrics represent corrections normalized to lie in σ space.

Application of Nonlinearity Metrics for Object 34943

We now apply these metrics to Object 34943 from Table 3. The fractional acceleration metric is shown in Figure 8 and both of the Mahalanobis metrics are shown in Figure 9. It is clear from any of these metrics that the corrections for this object become too large long before the same becomes evident from the correction magnitude itself. As early as 1 day into the propagation both the fractional acceleration and the Mahalanobis metrics indicate the problem while the correction distance remains only in tens of meters (see Figure 10). Nevertheless, we suggest that predictions after 1 day are unreliable. Incidentally, after 4 days the corrections become so large that the Object 34943 decays before reaching 5 day mark (Figure 11).

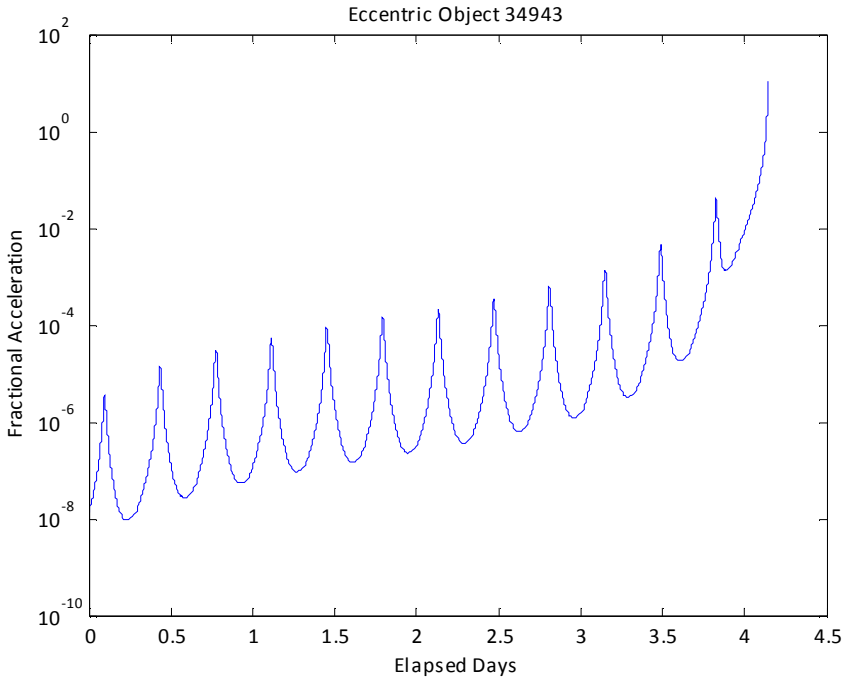

Figure 8. Fractional Acceleration Metric for Object 34943.

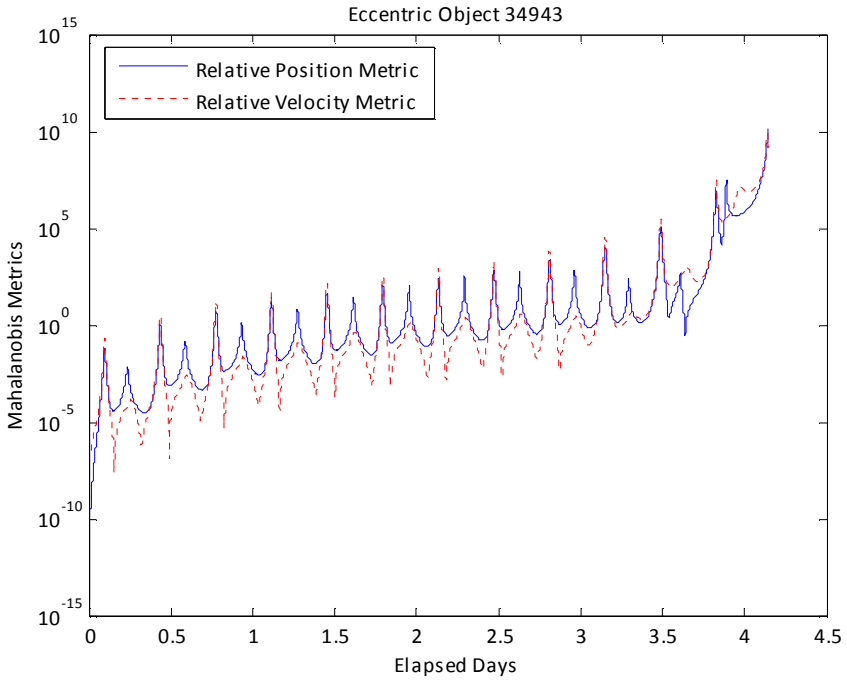

Figure 9. Mahalanobis Relative Position and Relative Velocity Metrics for Object 34943.

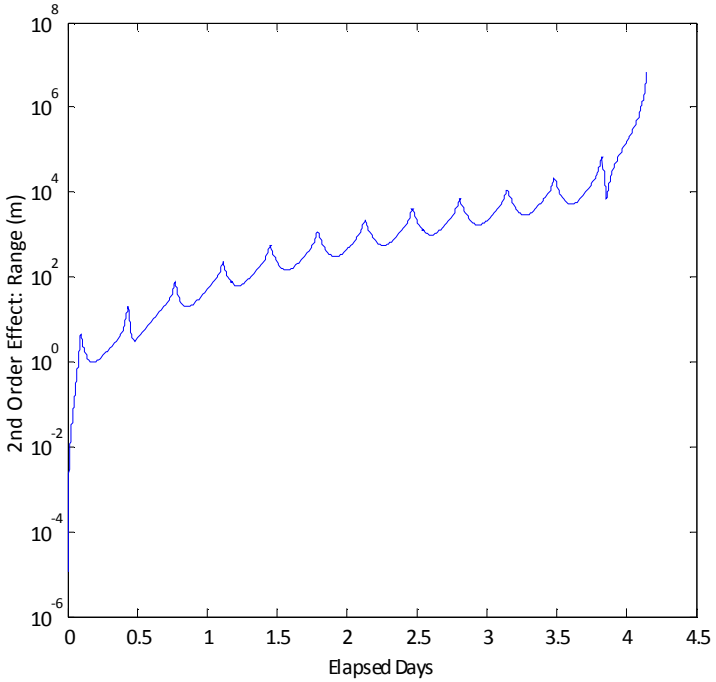

Figure 10. Correction Distance for Object 34943.

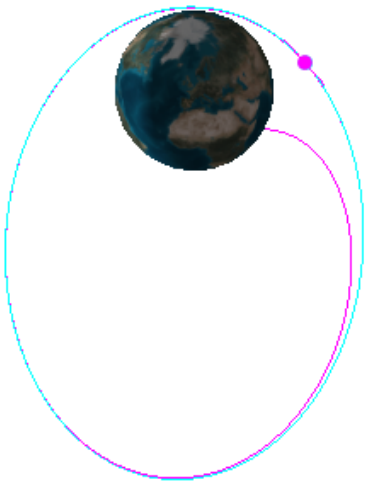

Figure 11. Final Reference and Corrected (Decaying) Orbits Object 34943.

Application of Nonlinearity Metrics for Objects 34712 and 35780

We also apply the same metrics to Objects 34712 and 35780 which we discovered to have a close approach event significantly affected by the second order correction (see Table 5). The fractional acceleration and the Mahalanobis metrics are shown in Figures 12 and 13 for the Eccentric Object 34712, and in Figures 14 and 15 for the LEO Circular Object 35780. The former exhibits a more substantial growth of all metrics compared with the latter. Nevertheless the metrics are significantly smaller than those of the exceptional Object 34943. In particular, at TCA the two objects have metrics shown in Table 6. Note that the close approach occurs near perigee of the eccentric object where the nonlinearity and the second order correction are high. However, because the nonlinearity metrics are reasonable for both objects, the corrected close approach may be considered more accurate.

Table 6. Nonlinearity Metrics Between Objects 35780 (LEO Circular) and 34712 (Eccentric) at TCA.

Nonlinearity Metrics	Eccentric Object 34712	LEO Circular Object 35780
Fractional Acceleration	6.74×10^{-6}	0.09×10^{-6}
Mahalanobis Position	0.70	1.01×10^{-4}
Mahalanobis Velocity	1.18	0.10×10^{-4}

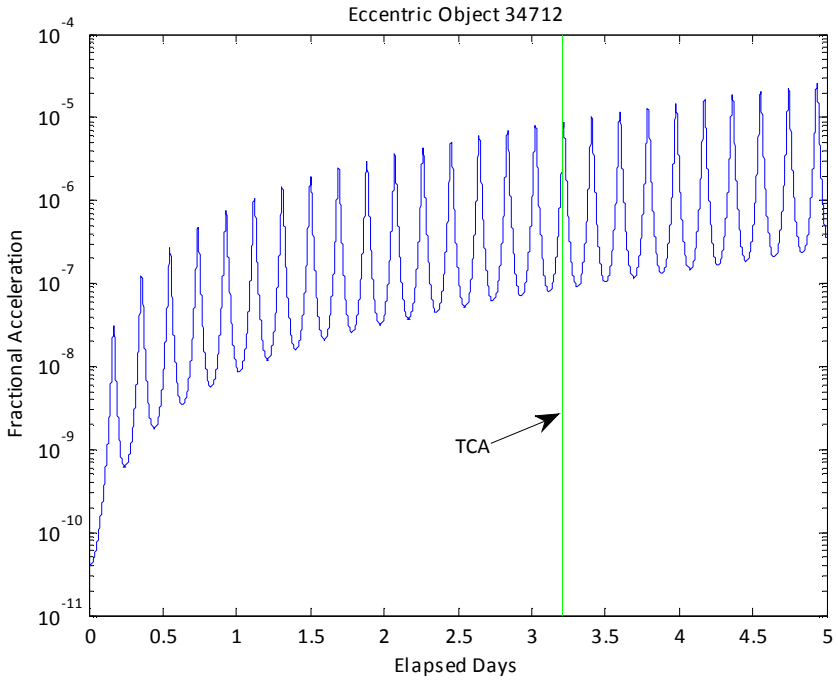

Figure 12. Fractional Acceleration Metric for Object 34712.

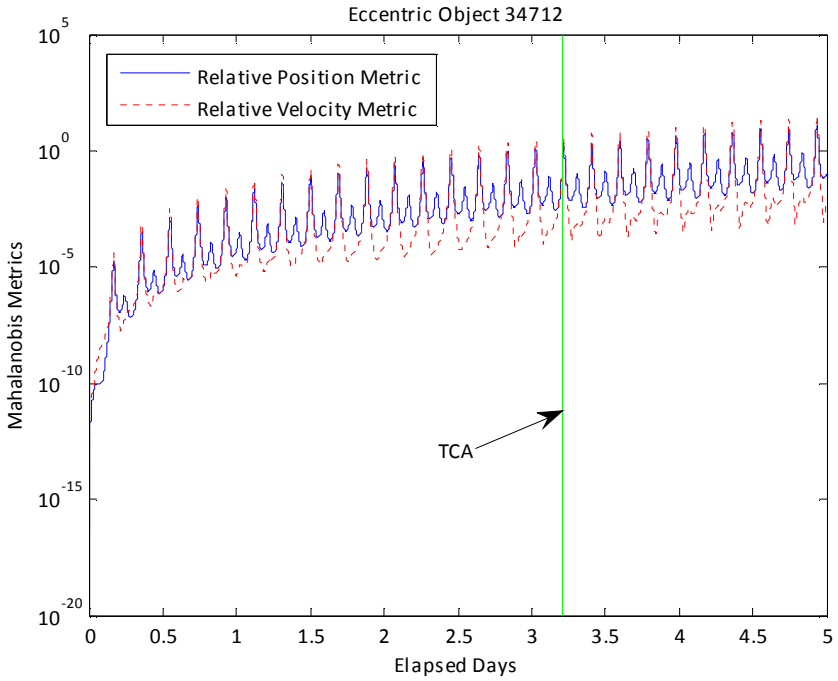

Figure 13. Mahalanobis Relative Position and Relative Velocity Metrics for Object 34712.

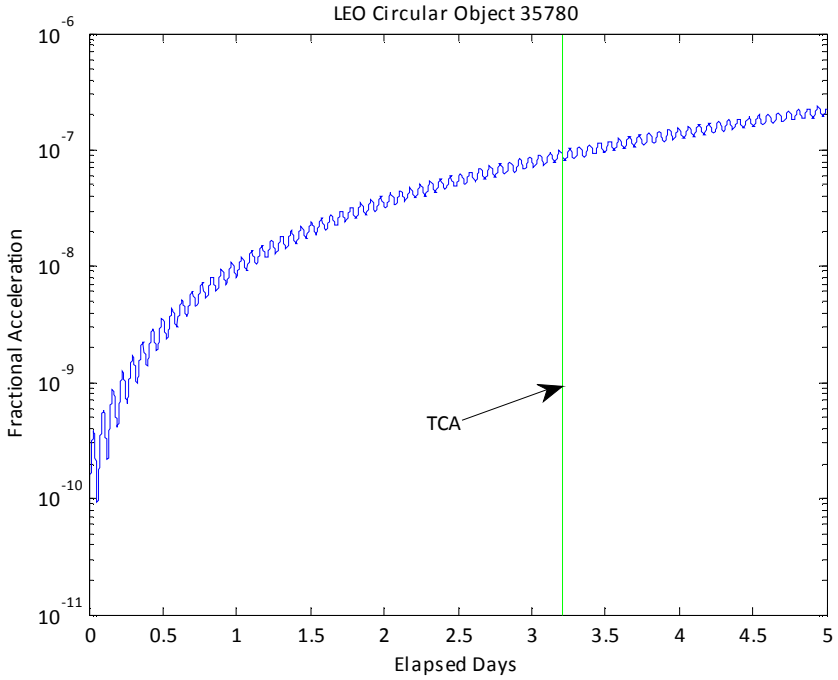

Figure 14. Fractional Acceleration Metric for Object 35780.

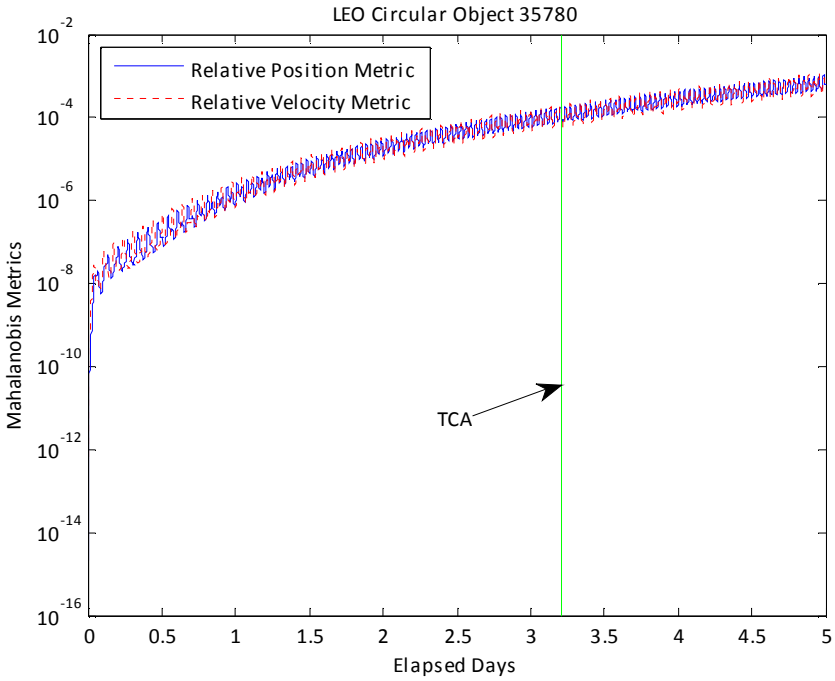

Figure 15. Mahalanobis Relative Position and Relative Velocity Metrics for Object 35780.

CONCLUSION

The process of generating predicted ephemerides for the entire space catalog was examined. Based on simulated initial state and error covariance data, it has been shown that long term predictions may become significantly affected by propagation nonlinearities. The second order effects interject the error covariance into the propagation of expected position and velocity resulting in the corrections that accumulate over time. The cumulative effect differs widely depending on the initial state and error covariance leaving some objects in the catalog largely unaffected for a long period of time while perturbing other objects relatively quickly and significantly. The time evolution of the correction generally passes through three stages: from initially unimportant, to significant for improving ephemeris accuracy, and, finally, to significant but only as an indicator of when the Gaussian assumptions about the distribution of ephemeris errors begin to breakdown and when further propagation and close approach analysis become imprudent. The conjunction events become affected inasmuch as the ephemerides of the objects involved are affected. In the simulated catalog, at least one event was found for which the second order corrections appear to improve accuracy and significantly affect characteristics of the event, miss distance in particular.

REFERENCES

[1] T.S. Kelso, “Analysis of the Iridium 33 – Cosmos 2251 Collision,” AAS 09-368, 2009 AAS/AIAA Astrodynamics Specialist Conference, Pittsburgh, PA, August 2009.

[2] V. Coppola, S. Dupont, K. Ring, and F. Stoner, “Assessing Satellite Conjunctions for the Entire Space Catalog using COTS Multi-core Processor Hardware,” AAS 09-374, 2009 AAS/AIAA Astrodynamics Specialist Conference, Pittsburgh, PA, August 2009.

[3] M. R. Akella and K. T. Alfriend, "Probability of Collision Between Space Objects," *Journal of Guidance, Control, and Dynamics,* Vol. 23, No. 5, September-October 2000, pp. 769-772.

[4] S. Alfano, "Satellite Collision Probability Enhancements," *Journal of Guidance, Control, and Dynamics*, Vol. 29, No. 3, May-June 2006, pp. 588-592.

[5] K. Chan, "Spacecraft Collision Probability for Long-Term Encounters," AAS Paper No. 03-549, AAS/AIAA Astrodynamics Specialist Conference, Big Sky, Montana, 3-7 August, 2003.

[6] S. Alfano, "Review of Conjunction Probability Methods for Short-term Encounters," AAS Paper No. 07-148, AAS/AIAA Space Flight Mechanics Meeting, Sedona, Arizona, 28 January-01 February 2007.

[7] R. P. Patera, "Satellite Collision Probability for Nonlinear Relative Motion," *Journal of Guidance, Control, and Dynamics*, Vol. 26, No. 5, 2003, pp. 728–733.

[8] D. A. Vallado, "A Preliminary Analysis of State Vector Prediction Accuracy," AAS 07-358, 2007 AAS/AIAA Astrodynamics Specialist Conference, Mackinac Island, MI, August 2007.

[9] D. A. Vallado, "An Analysis of State Vector Prediction Accuracy," Paper USR 07-S6.1 presented at the US/Russian Workshop, Monterey, CA, 2007.

[10] D. A. Vallado, "An Analysis of State Vector Propagation using Differing Flight Dynamics Programs," Paper AAS 05-199 presented at the AAS/AIAA Space Flight Mechanics Conference, Copper Mountain, CO, 2005.

[11] D. A. Vallado, and J. H. Seago, "Covariance Realism," AAS 09-304, 2009 AAS/AIAA Astrodynamics Specialist Conference, Pittsburgh, PA, August 2009.

[12] J. L. Junkins, M. R. Akella, and K. T. Alfriend, "Non-Gaussian Error Propagation in Orbital Mechanics," Vol. 44, No. 4, Oct.-Dec. 1996, pp. 541-563.

[13] R. S. Park and D. J. Scheeres, "Nonlinear Mapping Of Gaussian State Uncertainties: Theory And Applications To Spacecraft Control And Navigation," *Journal of Guidance, Control, and Dynamics*, Vol. 29, No. 6, pp. 1367-1375.

[14] S. Tanygin, "Examination of Non-linearity Based on the Second Order Expansion of the Orbit State Transition," AAS 09-412, 2009 AAS/AIAA Astrodynamics Specialists Conference, Pittsburgh, PA, August 2009.

[15] P. J. Huxel, and R. H. Bishop, "Navigation Algorithms and Observability Analysis for Formation Flying Missions," *Journal of Guidance, Control, and Dynamics*, Vol. 32, No. 4, July-August 2009, pp. 1218-1231.

[16] J. Woodburn, and S. Tanygin, "Detection of Non-Linearity Effects During Orbit Estimation," AAS 10-239, 2010 AAS/AIAA Spaceflight Mechanics Meeting, San Diego, CA, February 2010.